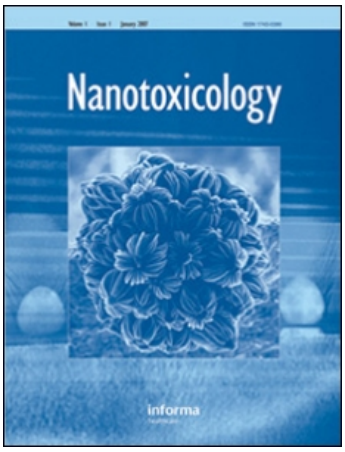


**Nanotoxicology**
Publication details, including instructions for authors and subscription information:
http://www.informaworld.com/smpp/title~content=t716100760

# Biodistribution and oxidative stress effects of a systemically-introduced commercial ceria engineered nanomaterial

Robert A. Yokel [ab]; Rebecca L. Florence [a]; Jason M. Unrine [c]; Michael T. Tseng [d]; Uschi M. Graham [e]; Peng Wu [f]; Eric A. Grulke [f]; Rukhsana Sultana [g]; Sarita S. Hardas [g]; D. Allan Butterfield [gh]
[a] Department of Pharmaceutical Sciences, [b] Graduate Center for Toxicology, [c] Department of Plant and Soil Sciences, [d] Departments of Anatomical Sciences & Neurobiology, University of Louisville, Louisville, Kentucky, USA [e] Center for Applied Energy Research, [f] Chemical & Materials Engineering Department, [g] Department of Chemistry, [h] Center of Membrane Sciences, University of Kentucky, Lexington, Kentucky

First Published on: 23 May 2009

**To cite this Article** Yokel, Robert A., Florence, Rebecca L., Unrine, Jason M., Tseng, Michael T., Graham, Uschi M., Wu, Peng, Grulke, Eric A., Sultana, Rukhsana, Hardas, Sarita S. and Butterfield, D. Allan(2009)'Biodistribution and oxidative stress effects of a systemically-introduced commercial ceria engineered nanomaterial',Nanotoxicology,3:3,234 — 248

**To link to this Article: DOI:** 10.1080/17435390902974496

**URL:** http://dx.doi.org/10.1080/17435390902974496

*Nanotoxicology*, September 2009; 3(3): 234–248

informa
healthcare

# Biodistribution and oxidative stress effects of a systemically-introduced commercial ceria engineered nanomaterial

ROBERT A. YOKEL[1,2], REBECCA L. FLORENCE[1], JASON M. UNRINE[3], MICHAEL T. TSENG[8], USCHI M. GRAHAM[4], PENG WU[5], ERIC A. GRULKE[5], RUKHSANA SULTANA[6], SARITA S. HARDAS[6], & D. ALLAN BUTTERFIELD[6,7]

[1]*Department of Pharmaceutical Sciences;* [2]*Graduate Center for Toxicology;* [3]*Department of Plant and Soil Sciences;* [4]*Center for Applied Energy Research;* [5]*Chemical & Materials Engineering Department;* [6]*Department of Chemistry;* [7]*Center of Membrane Sciences, University of Kentucky, Lexington, Kentucky &* [8]*Departments of Anatomical Sciences & Neurobiology, University of Louisville, Louisville, Kentucky, USA*

*(Received 19 January 2009; accepted 16 April 2009)*



**Abstract**

The objective was to characterize the biodistribution of nanoscale ceria from blood and its effects on oxidative stress endpoints. A commercial 5% crystalline ceria dispersion in water (average particle size $\sim 31 \pm 4$ nm) was infused intravenously into rats (0, 50, 250 and 750 mg/kg), which were terminated 1 or 20 h later. Biodistribution in rat tissues was assessed by microscopy and ICP-AES/MS. Oxidative stress effects were assessed by protein-bound 4-hydroxy 2-*trans*-nonenal (HNE), protein-bound 3-nitrotyrosine (3-NT), and protein carbonyls. Evans blue (EB)-albumin and Na fluorescein ($Na_2F$) were given intravenously as blood-brain barrier (BBB) integrity markers. The initial ceria $t_{½}$ in blood was $\sim$7 min. Brain EB and $Na_2F$ increased some at 20 h. Microscopy revealed peripheral organ ceria agglomerations but little in the brain. Spleen Ce concentration was >liver >blood >brain. Reticuloendothelial tissues cleared ceria. HNE was significantly increased in the hippocampus at 20 h. Protein carbonyl and 3-NT changes were small. The nanoparticle characterizations before and after biodistribution, linked with the physiological responses, provide a foundation for evaluating the effects of engineered nanomaterial physico-chemical properties on peripheral organ distribution, brain entry and resultant toxicity.

**Keywords:** *Blood-brain barrier, ceria, neurotoxicity, oxidative injury, rat*

**Abbreviations:** AES, atomic (optical) emission spectrometry, BBB, blood-brain barrier, Ce, ceria, EB, Evans blue, EM, electron microscopy, ENM, engineered nanomaterial, ICP, inductively-coupled plasma, MDL, method detection limit, MS, mass spectrometry, HNE, 4-hydroxy-2-*trans*-nonenal, 3-NT, 3-nitrotyrosine, RES, reticuloendothelial system, RNS, reactive nitrogen species, ROS, reactive oxygen species, RPD, relative percent difference, SD, standard deviation, XRD, X-ray diffraction.

## Introduction

The emergence of nanotechnology over the past two decades has presented seemingly unlimited opportunities in many fields; however, information about toxicology has lagged far behind. The complexity of this newly emerging area of investigation poses serious challenges for scientific investigations that rely solely on the perspectives of traditional disciplines. An engineered nanomaterial (ENM) that solves an important problem in the engineering or environmental fields (i.e., ENMs for bioremediation) may have serious consequences after unintended uptake by humans. Inadequate identification of ENM hazards and management of risks from exposure could lead to serious human health problems (Nel et al. 2006). Engineered nanomaterials that exist as discrete, submicron particles are particularly worrisome. Their small sizes (comparable to DNA [2.5 nm] and large proteins [albumin 7.2 nm]) make it physically possible for the nanoparticle to migrate through capillaries, cell membranes and cell substructures, and their enormous surface area to mass ratios may expose highly reactive sites, such as specific crystal surfaces, edges or corners, to local

Correspondence: Robert A. Yokel, PhD, Department of Pharmaceutical Sciences, 511C Pharmacy Building, 725 Rose Street, University of Kentucky Academic Medical Center, Lexington, KY, 40536-0082, USA. Tel: +1 859 257 4855. Fax: +1 859 323 6886. E-mail: ryokel@email.uky.edu

ISSN 1743-5390 print/ISSN 1743-5404 online 
DOI: 10.1080/17435390902974496

environments in the body (Oberdörster et al. 2005b; Davies 2006; Maynard 2006). ENM properties thought to influence their pharmacokinetics and toxicity are: (i) Particle size and distribution (Mamot et al. 2004; Lovric et al. 2005; Gao and Jiang 2006), (ii) agglomeration (Jakupec et al. 2005), (iii) shape, and (iv) surface properties, such as (a) area compared to particle size, (b) porosity, (c) charge [zeta potential] (Fenart et al. 1999; Brigger et al. 2004; Lockman et al. 2004), (d) surface chemistry [coating], (e) chemical composition, (f) crystallinity and (g) reactivity. Biopersistence and re-distribution within the organism also influence ENM pharmacokinetics and toxicity (Ferin et al. 1990, 1992; Kreyling et al. 2002; Semmler et al. 2004; Oberdörster et al. 2005b). There is little information about the toxicology of ENMs. There is a need to determine the influence of the physico-chemical properties of ENMs on their distribution into and across the blood-brain barrier (BBB) and into brain cells, compared to peripheral organs, and their beneficial and/or hazardous effects on these organs.

Many ENMs are comprised primarily of metals and oxides of Al, Ce, Cu, Au, Fe, Pd, Si, Ag, Ti and Zn. Ceria (a.k.a.: $CeO_2$, ceric oxide, Ce dioxide, Ce oxide, CAS # 1306-38-3) was selected for the present studies to characterize ENM biodistribution from blood and its effects on oxidative stress endpoints because: (1) It is an insoluble metal oxide that can be readily observed *in situ* by electron microscopy (EM), making it a useful *in vivo* tracer, (2) it is redox reactive (Zhang et al. 2004), (3) it can be functionalized (e.g., Qi et al. 2008), (4) it is available in sizes relevant for uptake across the BBB, one of the most limiting mammalian membranes, (5) it can be produced in a variety of shapes by many different methods, including nanodisks, nanoplates, nanotubes, nanocubes, nanorods, nanopolyhydra, and tadpole, comet, and prism shapes (Mai et al. 2005; Si et al. 2005; Yu et al. 2005; Bai et al. 2006; Han et al. 2006; Yang and Gao 2006), and (6) it has current commercial applications. A major commercial application of ceria is its use as an abrasive for chemical-mechanical planarization of advanced integrated circuits. This application of ENMs accounted for 60% of the $1 billion market for nanomaterials in 2005 (Feng et al. 2006). Another significant application is its use as a catalyst in ENMs that have very small size, large surface area, thermal stability to 650°C and are stable in humid air (Trovarelli 2002). For example, ceria (10 nm primary particles coated with a dispersant to facilitate its dispersion in fuel liquids) is marketed by Oxonica Ltd. as Envirox®, a diesel fuel catalyst to improve combustion, reduce fuel consumption and decrease exhaust emissions (UK MNT Network).

Ceria was also considered to be a good candidate for these studies because it has been reported to have both pro-oxidant and anti-oxidant properties (see the *Discussion* section). These properties represent the conundrum enveloping the development of ENMs: There is evidence for both beneficial and toxic effects to the same organ, the brain.

Both the ILSIRF/RSI expert working group and the National Cancer Institute Nanotechnology Characterization Laboratory highlighted three key elements for a toxicity screening strategy of ENMs: (1) Physico-chemical characteristics, (2) cellular and non-cellular *in vitro* assays, and (3) *in vivo* assays. 'Tier 1 evaluations' of these groups included markers of inflammation and oxidant stress in selected remote organs and tissues such as the nervous system (Oberdörster et al. 2005a). Nanoscale ceria has been nominated by the NIEHS for toxicological consideration, including toxicokinetic studies, due to its widespread and expanding industrial uses, limited toxicity data, and a lack of toxicological studies for nanoscale ceria (Integrated Laboratory Systems 2006).

The primary anticipated routes of human exposure to ENMs intended for industrial or environmental applications include inhalation exposure, dermal uptake, and oral ingestion with possible subsequent absorption of ENMs into systemic circulation. Translocation from the lung to systemic organs, particularly the liver, has been seen with nanoscale silver (Takenaka et al. 2001), $^{192}$Ir (Kreyling et al. 2002), $^{99m}$Tc-labeled carbon (Nemmar et al. 2002) and 20–29 nm $^{13}$C particles (Oberdörster et al. 2002), although the percentage of the dose found in internal organs was small. There appears to be no reports of skin penetration of ENMs $\leq$10 nm and no evidence that ENMs $\geq$20 nm penetrate healthy skin (Warheit et al. 2007). There is considerable interest in ENMs to enhance drug delivery to the brain, as reviewed by Koziara et al. (2006). Although some data exist on the absorption properties and associated toxicities of ENMs after exposure via the pulmonary, oral, and topical routes, little is known about their distribution into the brain once they reach systemic circulation. As stated in a review of the risks of industrial nanomaterials, 'The effect of nanomaterials on organs "inside" the body (e.g., liver and brain) and the blood have been studied from the few publications on the permeation of nanomaterials through the lung, skin, or intestinal barrier ...' (Luther 2004).

The objectives of the present research were to determine: (1) The distribution of ceria ENMs from systemic circulation into the BBB, brain, and selected peripheral organs, and (2) the resultant

selected effects, including histopathology and pro- or antioxidant effects. The intravenous route of exposure was used to assess the potential for the model ENM, after being absorbed by any route and entering systemic circulation, to distribute into organs and produce toxicity.

## Methods

### *Materials*

*Nanomaterial.* A 5% ceria dispersion in water at pH 4.2 (Aldrich #639648; USA) was used. The specifications for this product were: <150 nm and a 4.5–5.5% dispersion. The physical properties of nanoparticles reported by the manufacturer are not always the actual properties of a particular lot.

*Ceria characterization.* The ceria dispersion was opaque, suggesting that some particles were larger than 100 nm. Therefore, the physical properties of this sample were determined in our laboratory: TEM for primary particle morphology, dynamic light scattering to evaluate agglomeration and ζ-potential to determine dispersion stability. Fourier transform infra-red spectroscopy (FTIR) studies were conducted to ascertain whether this ENM had been surface stabilized. X-ray diffraction (XRD) was conducted to obtain information on the crystal lattice parameters and crystallite sizes of the ceria ENM. The XRD patterns were scanned from 20–90° 2 theta range using 0.02° step intervals.

For these studies the commercial product (10 ml) was sonicated for 3 min (0.5 inch probe, Dr Hielscher GmbH UP400S Ultraschallprozessor, 0.5 sec on/0.5 sec off, 50% power). To determine if the sonicator probe released metals into the ceria dispersion, samples of unsonicated ceria dispersion and four aliquots of sonicated dispersion, two obtained from an infusion syringe after completion of ceria infusion to rats, two that had not been placed in a syringe, were analyzed by ICP-MS. Osmotic strength was measured using a Fiske One-Ten Freezing Point Osmometer and found to be ~30 mOs. To avoid intravenous administration of a considerable volume of a grossly hypotonic ceria dispersion, the potential to use saline or 10% sucrose as a vehicle was assessed. Primary ENM size and structure were determined using HR-TEM and HR-STEM. Additional information about crystal structure was obtained using electron diffraction in TEM mode.

*Ceria characterization results.* Particle size determination was conducted by dynamic light scattering (DLS: Brookhaven Instruments Limited 90Plus NanoParticle Size Distribution Analyzer). The ceria dispersion was not transparent at the original concentration (5 wt%) and was diluted 1:500 with distilled water with sonication. This dispersion was optically clear and suitable for DLS evaluation. The number-average particle size distribution showed that the average particle size was $31 \pm 4$ nm (consistent with the transparency of the dispersion), and ~99% of the particles were in a fairly narrow range. If the nanoparticles were platelets, then the exact diameter would have to be estimated by modifying the light scattering calculations using shape correction factors. This average diameter seems consistent, and should be, with the particle sizes observed by HRTEM (Figure 1). Volume-average particle size diameters were also estimated by light scattering (this method is more indicative of the mass of the particles in specific fractions, and emphasizes larger particles). The volume-based PSD was bimodal, with one peak centered near 31 nm (~77 mass%), and a second peak centered near 160 nm (~23 mass%). For these data, the correlation function was good, i.e., insufficient agglomeration occurred during the analysis time (15 min) to affect the distributions. These results are typical of seven different samples.

The particle size distribution of this sample was analyzed using TEM and software (Digital Micrograph). The sample had a bimodal distribution, with peaks having average particle sizes of 8 and 24 nm. There were some particles in this sample ~100 nm. HRTEM analysis of the sample (Figure 1) shows that the nanoparticles were highly crystalline (illustrated by the uniform lines in the particle that demonstrate aligned atoms), and that most of the particles were platelets. Given that the ceria nanoparticles were platelets that did not have a monodisperse particle size distribution, the typical equation relating surface area of spherical particles to their average diameter would not be accurate.

Zeta potential measurements of the dispersion, from a Malvern 2000 zetasizer, showed that the system was unstable ($-7.6 \pm 3.7$ mV) at its original pH (4.2), but that the system should be stable at physiological pH (−35 mV at pH 7.4). Acetic acid and potassium hydroxide were used to control pH. Therefore, the dispersion was not stable and would be expected to agglomerate. Agglomerated material could be dispersed by sonication, which was applied prior to infusions and other operations.

Taking the HRTEM and light scattering data together, this ceria sample had particles with one dimension in the order of 31 nm. Both light scattering and zeta potential results suggest that agglomeration can occur in the as-received sample.

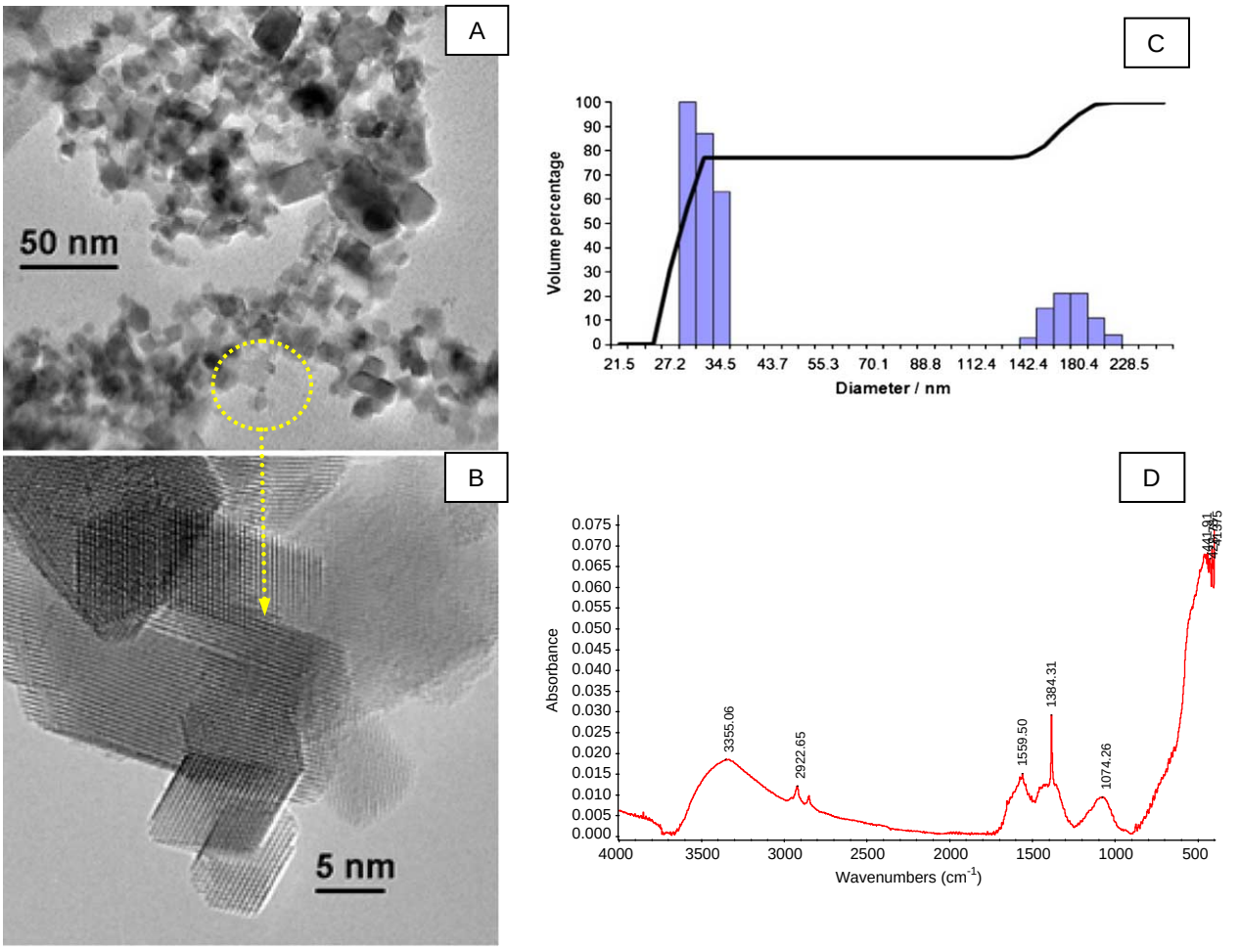


Figure 1. HRTEM results for the ultrasonicated 5% ceria ENM dispersion used in this study. Panel A: Lower magnification showing particle size distribution. The upper limit of the particle size range was ~100 nm. Panel B: Higher magnification illustrating that the lower limit of the particle size range was ~5 nm. All size fractions of the ceria ENM were highly crystalline. Panel C: The volume-based particle size distribution was bimodal. Panel D: FTIR scan of the powder surface showed the presence of carboxylate groups.



### *Agglomeration assessment*

The effect of saline and 10% sucrose on agglomeration of this ceria ENM was assessed *in vitro* by their individual addition to a 5% dispersion, followed by repeated particle size determination. These caused sufficient ceria ENM agglomeration to discourage their use as vehicles to prepare an iso-osmotic ceria dispersion. In the absence of a suitable agent to raise the osmotic strength of the ceria dispersion, it was administered to the rats in water.

To predict ceria ENM agglomeration *in vivo*, freshly drawn whole rat blood was incubated with the ceria ENM (0.14, 0.7 and 3.56 mg ceria/ml) for 1 h, allowed to clot, fixed in formalin, and processed for high resolution transmission electron microscopy, scanning TEM, and energy-dispersive X-ray spectroscopy.

### *Animals*

This study used 52 male Fisher 344 rats, weighing 275 ± 25 g (mean ± SD) that were housed individually prior to the study in the University of Kentucky Division of Laboratory Animal Resources facility. Animal work was approved by the University of Kentucky Institutional Animal Care and Use Committee. The research was conducted in accordance with the Guiding Principles in the Use of Animals in Toxicology.

### *Ceria pharmacokinetics and distribution*

Rats were surgically prepared with two intravenous cannula that were inserted into femoral veins and terminated in the vena cava. The next day the unanesthetized rats were assigned to be infused

intravenously with ceria in water via one (the shorter) cannula concurrently with an equal volume and rate of 1.8% saline infused into the second cannula. Each fluid was delivered at the rate of ~0.6 ml/h. Nineteen rats were infused with 0 ($n=4$; 1 infused 0.5 h, 2 infused 2.5 h and 1 infused 7.5 h), 50 ($n=5$), 250 ($n=5$) or 750 ($n=5$) mg ceria/kg and terminated $1.080 \pm 0.001$ h (mean $\pm$ SD) after completion of the infusion and 32 rats were infused with 0 ($n=10$; two infused 0.5 h, 4 infused 2.5 h and 4 infused 7.5 h), 50 ($n=7$), 250 ($n=7$) or 750 ($n=8$) mg ceria/kg and terminated $20 \pm 4$, (mean $\pm$ SD) h after completion of the infusion. Therefore the 50, 250 and 750 mg ceria/kg doses were achieved by infusion durations of 0.5, 2.5 and 7.5 h. Blood was repeatedly withdrawn from some rats after completion of ceria infusion for up to 240 min. One or 20 h after completion of the ceria or vehicle infusion the rats were anesthetized with ketamine, dosed with BBB integrity markers described below, given additional ketamine if necessary and decapitated to rapidly harvest the brain and other organs. Post-mortem samples were obtained to determine the Ce concentration in brain, liver, spleen and blood by ICP-AES/ICP-MS. The weight of the brain, liver, spleen and a kidney were determined in all rats that were terminated 1 h after the infusion and in 6, 3, 3, and 6 rats terminated 20 h after 0, 50, 250 or 750 mg/kg ceria infusions (except not brain) to enable a mass balance determination of the ceria in the brain, liver and spleen, as the product of tissue [Ce] $\times$ organ weight. To estimate the percentage of the ceria dose in the blood, blood [Ce] was multiplied by the rat's weight $\times$ 7%, the average blood volume of the rat (Wang and Hegsted 1949).

To prepare for Ce analysis tissue, blood and serum were dried, digested in a 2:1 $HNO_3$:$H_2O_2$ mixture + 2% $H_2SO_4$, the liquid evaporated, and the residue reconstituted in 2% $HNO_3$. Ce was initially analyzed by ICP-AES (Thermo Jarrell Ash IRIS Advantage Dual View). The instrument detection limit (IDL) was determined following US EPA 2002 guidelines, as follows. The IDL was estimated, a laboratory standard was prepared at that concentration and analyzed on three non-consecutive days and the IDL calculated from the SD of seven replicates and the *t*-value of 3.143 for 99% confidence level. The IDL was 0.008 mg Ce/l. Spike recovery for ICP-AES analyses ranged from 96–104%. Each sample was analyzed $\geq 2$ times. The relative standard deviation of 95% of the samples was $<10$, the RSD of the remaining 5% of the samples was $>10$ and $<20\%$. One sample was $>20\%$ and was not included in the data analysis. Samples below the IDL for ICP-AES were analyzed by ICP-MS (Agilent 7500cx) using external calibration and 5 ng terbium as an internal standard. Spike recovery for ICP-MS analyses was $94 \pm 3\%$ (mean $\pm$ SD). Average relative percent difference between replicate analyses was $3.2 \pm 2.0\%$. The IDL ranged from 13–63 ng/L. Based on the average wet weight of tissue (44 mg) and blood or serum (214 mg), dilution of the digested sample to 15 ml for ICP-AES and 30 ml for ICP-MS, and an MDL for acid digestion blanks assayed by ICP-MS, calculated as three times the SD of the blanks of 0.0039 mg Ce/l, the MDLs for tissue and blood or serum samples analyzed by ICP-MS were 0.089 mg Ce/kg and 0.018 mg Ce/l, respectively. Based on the IDL of 0.008 mg Ce/l for ICP-AES, the 44 and 214 mg wet weight of tissue and blood or serum produce detection limits of 2.73 and 0.56 mg ceria/kg or l, respectively. Values below the MDL were assigned a value of ½ of the MDLs for data analysis.

### *Blood-brain barrier integrity assessment*

Five min before termination the anesthetized rat was given Na fluorescein (334 $D_a$) and Evans blue (EB: ~67,400 $D_a$ when bound to albumin) as small and large BBB permeability markers, respectively. These were given intravenously in saline to deliver in 1 ml/0.3 kg rat, 20 mg EB that had been incubated overnight with 18 mg albumin and 6 mg Na fluorescein. The doses were based on prior work (Uyama et al. 1988; Kabuto et al. 1997; Hawkins and Egleton 2006). Post-mortem brain samples were obtained to quantify EB and fluorescein. Each brain sample was homogenized in 3 ml 7.5% trichloroacetic acid then divided into two equal aliquots. To one aliquot was added an equal volume of water, then 250 µl of 5 N NaOH (which we found in preliminary studies to be more than required to produce the highly alkaline solution that converts fluorescein to a fluorophore). This was quantified by fluorometric spectroscopy (ex. 492 nm, em. 514 nm), compared to standards in the same matrix. The other sample was centrifuged at 10,000 *g* at 4°C for 10 min and EB determined by visible spectroscopy at $\lambda_{max}$, 609 nm compared to standards in the same matrix.

### *Oxidative stress assessment*

Post-mortem samples were rapidly obtained and frozen in liquid nitrogen for later determination of markers of protein oxidation in cortex, hippocampus, and cerebellum. Three endpoints were studied: (1) Protein carbonyls (a product of reactive oxygen and nitrogen species [ROS] oxidation of protein

amino acid side chains, e.g., Lys, Arg, Pro, Thr and His; peptide backbone scission; Michael addition reactions of His, Lys and Cys residues with products of lipid peroxidation; or glycoxidation reactions; (2) 3-nitrotyrosine (protein-bound 3-NT; a covalent protein modification from the action of RNS on the *ortho* position of the aromatic ring of tyrosine residues in proteins); and (3) protein-bound (HNE; a product of lipid peroxidation of polyunsaturated omega-6 acyl groups, such as arachidonic, or linoleic groups on glycerophospholipids and corresponding fatty acids). Each parameter was determined by the slot-blot technique with specific antibodies (Butterfield 1997; Sultana et al. 2005). Each sample was analyzed in duplicate, and compared to samples from control rats processed in the same analysis.

### *Light and electron microscopic assessment of ceria ENM localization*

Post-mortem liver, spleen, kidney and brain samples were stored in 10% neutral buffered formalin then processed for light microscopic (LM) and electron microscopic (EM) localization of ceria ENMs and histopathology assessment. A Philips CM 10 electron microscope was used.

### *Data and statistical analysis*

All results are expressed as mean $\pm$SD. Brain fluorescein and EB concentrations were calculated for each rat that received ceria as a percentage of rats in the same squad (conducted at the same time) that did not receive ceria. Levels of brain-resident protein carbonyls, 3-NT and protein-bound HNE concentrations were calculated for rats that received ceria as a percentage of these same parameters in brain from rats in the same squad (analyzed at the same time) that did not receive ceria.

RSTRIP, a pharmacokinetic data stripping program, was used to estimate the initial half-life of ceria clearance from blood after termination of the ceria infusion (Fox and Lamson 1989).

One-way ANOVA tests were conducted to compare organ weights normalized to body weight, the Ce concentration in tissues, and brain EB and fluorescein from control and treated rats, followed by Tukey's Multiple Comparison Test when the ANOVA was significant. One-way ANOVA tests were conducted to compare carbonyls, protein-bound HNE and 3-NT in the brain of treated compared to control rats, followed by Dunnett's Multiple Comparison Test when the ANOVA was significant. $P$ values $<0.05$ were considered significant.

## Results

Light scattering particle size determinations suggested the mean ceria ENM size was $\sim$30 nm, which correlated with HR-TEM imaging of the dosing material (Figure 1). The zeta potential was $-7.6 \pm 3.7$ mV at pH $\sim$4.2, suggesting that the dispersion was unstable. FTIR results showed several peaks between 1300 and 1700 $cm^{-1}$ indicating the ceria ENM was modified with organic molecules, probably either an intentionally added stabilizer or an unintentional contaminant. The exact nature of this organic matter was not determined. Bragg peaks obtained from the XRD results showed the presence of pure ceria in a cubic lattice with corresponding Miller indices of (111), (220) and (311), and with lesser presence of (200), (222) and (400). Additional Bragg peaks at (331) and (420) were also present, although having rather low intensity.

ICP-MS analysis of unsonicated ceria dispersions showed the presence of lead, aluminum, copper and titanium at quantifiable concentrations (23.5, 10.2, 4.4 and 3.2 mg/kg). Iron, nickel and zinc were below quantifiable concentrations (6.5, 0.5 and 12 mg/kg, respectively). Therefore, the sum of the contamination from lead, aluminum, copper, titanium, iron, nickel and zinc was $<0.2\%$ of the Ce concentration. There were no consistent differences in metal concentrations in dispersions that had been in syringes *vs.* those that had not. Titanium was the only metal that sonication increased, to $\sim$34 mg/kg, or $\sim 0.1\%$ of the Ce concentration.

Addition of sodium chloride (to a final concentration of 0.9%) to the ceria ENM aqueous dispersion caused rapid ceria agglomeration. After 5 min, the agglomerate particle sizes ranged from 240–430 nm; after 40 min, 98% of the agglomerates were 270–480 nm with 2% $>2$ μm (number fraction basis). One h after addition of sucrose (to a final concentration of 10%), the agglomerate size distribution was multimodal, with peaks near 60 nm (82%), 160–240 nm (16%) and 405–480 nm (2%). After $\sim$20 h, $\sim$89% of the agglomerates were between 110 and 140 nm and $\sim$11% were between 330 and 440 nm. Blood incubated with ceria ENM for 1 h had agglomerates ranging from $\sim$200 nm to $>1$ μm (Figure 2). The presence of Ce was verified by energy-dispersive X-ray spectroscopy in one of the agglomerates (Figure 2).

The initial $t_{1/2}$ of ceria clearance from blood after termination of the infusion was very rapid (Figure 3), and was calculated to be 7.5 min, based on the 250 mg ceria/kg dose. When blood was centrifuged, at 1600 *g* for 10 min, to generate plasma, nearly 75%

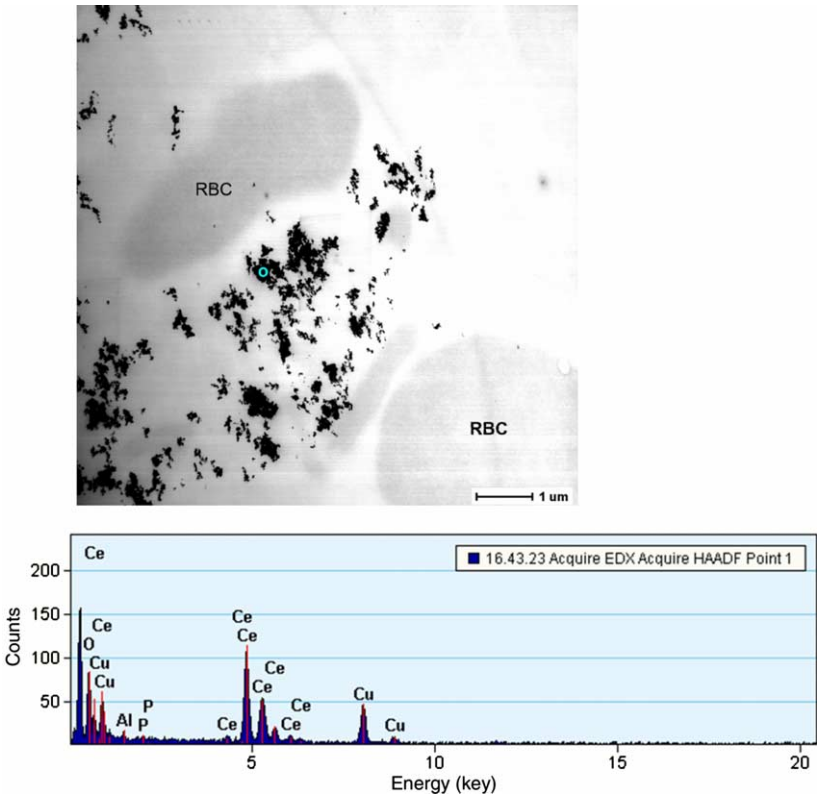


Figure 2. Upper panel: STEM image of blood incubated with ceria ENMs for 1 h. Ceria agglomerates were seen between two RBCs (erythrocytes). The circle indicates the placement of the EDX probe. Lower panel: Energy-dispersive X-ray spectroscopic image of circled area in the upper panel showing the presence of Ce. This was obtained using a STEM high angle angular dark field detector (HAADF).



of the suspended ceria appeared in a pellet on the bottom of the tube. Therefore the relative concentrations of Ce in plasma vs. whole blood shown in Figure 3 should not be interpreted as the relative ceria distribution between these two compartments.

During the intravenous ceria infusion, clinical toxicity was limited to slight tachypnea and dyspnea that were only observed in rats that received 750 mg ceria/kg, bruxism and excessive licking in some rats that received all doses, and chewing the floor grate and reaching through the grate to eat wet bedding in some rats that received 750 mg ceria/kg. The intravenous infusion of one rat was terminated prior to its target of 7.5 h, at 5.86 h (586 mg ceria/kg), due to these signs. No adverse effects were seen after completion of the intravenous infusion. No animals died prior to their planned termination.

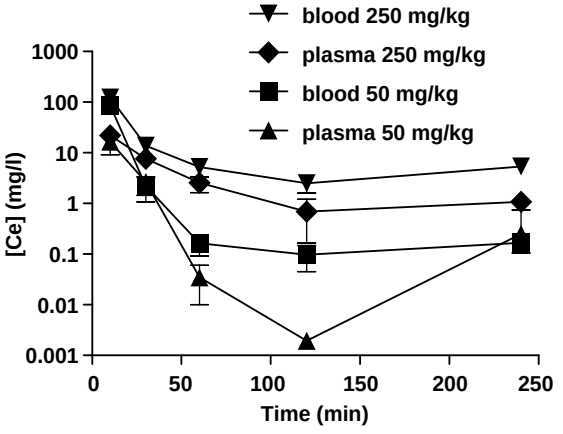


Figure 3. Blood and plasma Ce concentrations, determined by ICP-AES/ICP-MS, after completion of intravenous ceria ENM infusion. Results are mean ± SD of 4 rats at each dose.

Kidney and liver weights increased as a function of ceria dose. When normalized to body weight, kidney weights in the 750 mg ceria/kg treated rats terminated at 20 h were greater than the control group and liver weights in the 750 mg ceria/kg treated rats terminated at 20 h were greater than the control, 50 and 250 mg ceria/kg groups.

Tissue Ce concentration was ceria dose-dependent. The Ce concentration was highest in the spleen, which was higher than the liver, which was higher than the brain (Table I). One and 20 h after completion of the ceria infusion organ weight × Ce concentration showed the liver, spleen, blood and brain had ~37, 3, <0.5, and <0.002% (1 h) and ~57, 16, 0.2–4, and 0.01–0.02% (20 h) of the infused ceria, respectively.

Table I. Blood and tissue Ce concentration 1 and 20 h after completion of intravenous ceria infusion.

| | Cerium (mg/i or mg/kg wet weight) | | | |
|---|---|---|---|---|
| Ceria dose (mg/kg) | Blood | Brain | Liver | Spleen |
| 1 h termination | | | | |
| 0 | 0.032±0.045 | 0.12±0.09 | 0.25±0.31 | 0.57±0.95 |
| 50 | 0.56±0.50 | 0.087±0.067 | 390±137 | 544±266 |
| 250 | 1.3±1.4 | 0.15±0.10 | 1632±941[a,b] | 1994±1171 |
| 750 | 41±11[a,b,c] | 1.1±0.3[a,b,c] | 6327±725[a,b,c] | 11350±2185[a,b,c] |
| 20 h termination | | | | |
| 0 | * | * | * | * |
| 50 | 1.2±0.1 | 1.0±0.3 | 610±131 | 2828±589 |
| 250 | 13±0 | 3.4±1.0[a,b] | 3139±1528[a,b] | 9237±1452[a,b] |
| 750 | 354±45[a,b,c] | 7.4±1.2[a,b,c] | 9335±1451[a,b,c] | 32752±5065[a,b,c] |

*All were below the limit of detection. [a]Different from 0 mg/kg ceria dosed rats (controls). [b]Different from 50 mg/kg ceria dosed rats. [c]Different from 250 mg/kg ceria dosed rats.

Ceria agglomerations were seen in the spleen red pulp at 1 h but not in the white pulp (which consists of lymphatic nodules and diffuse lymphatic tissue) (Figure 4, panel A). Similarly red pulp from the 20 h rats showed considerable ceria accumulation. These were intracellular accumulations, presumably by macrophages. Electron microscopic analysis indicated cytoplasmic localization without specific nuclear or mitochondria affiliation. No obvious histopathology was seen in the spleen. Intracellular ceria agglomerations were seen in Kupffer cells and hepatocytes (Figure 4, Panels B and C). The Kupffer cells were enlarged, accommodating the intracellular agglomerations. Some histopathology was seen in hepatocytes in rats that received 250 mg ceria/kg and were terminated at 20 h. More cells were affected in rats that received the 750 mg/kg dose, as shown in Figure 4, Panel C. Electron micrographs revealed intracellular ceria ENM in the kidney (Figure 4, Panel D).

Additionally, accumulations of ceria were seen in the afferent arterioles leading into glomeruli in rats given 750 mg ceria/kg. It is not known if these were extra- or intracellular. Similar accumulations were not observed in the liver or spleen. Some histopathology was seen in the kidney in 250 and 750 mg/kg dosed rats terminated 20 h after the infusion. Some epithelial lining in proximal convoluted tubules became distended with proteinacious material. Cytoplasmic protein globules in cells of the proximal convoluted tubules were observed in a few of the 750 mg/kg treated rats 20 h after exposure. However, renal corpuscle swelling was not observed. The ceria infusion produced a dose- and time-dependent increase of activated Kupffer cells, which were not seen in the control rats (Figure 5). In contrast to the significant accumulation of ceria agglomerations in reticuloendothelial organs, much less ceria was seen in the brain (Figure 6), consistent with the much lower Ce concentration in this organ compared to the spleen, liver and kidney (Table I). No microscopic evidence of disruption of the BBB was observed.

Brain fluorescein and EB in ceria-dosed rats were not significantly different from control rats 1 h after ceria infusion (Figure 7, upper panel). Twenty h after completion of the ceria infusion, fluorescein and EB were elevated, although generally not reaching statistical significance (Figure 7, lower panel).

There were no significant changes in the oxidative stress markers (protein-bound HNE, protein-bound 3-NT and protein carbonyls) in rats terminated 1 h after completion of the ceria infusion (Figure 8, upper panel). Rats terminated 20 h after the ceria infusion showed a significant increase of protein-bound HNE in the hippocampus and a decrease of protein carbonyls in the cerebellum (Figure 8, lower panel).

## Discussion

Material characterization results we obtained were not fully consistent with the properties of this commercial ENM provided by its supplier. FTIR results suggested it had an unknown, and not revealed (for proprietary purposes), surface stabilizer(s). Surface stabilizers are commonly added to ENM to provide ease of dispersion. However, in an adverse effects assessment, as in this study, the presence of unknown components of the study material is not desired. To avoid this confound in future studies, we are preparing materials to have precise control over surface coating effects in our future studies. The commercial ceria ENM used in this study was quite pure in regards to other metals. Sonication added little metal to the ceria. The low ratio of non-cerium metals to ceria suggests that effects seen in this work are due to the ceria ENM.

The size of the ceria ENM utilized in the present study was larger than the ceria added to diesel fuel

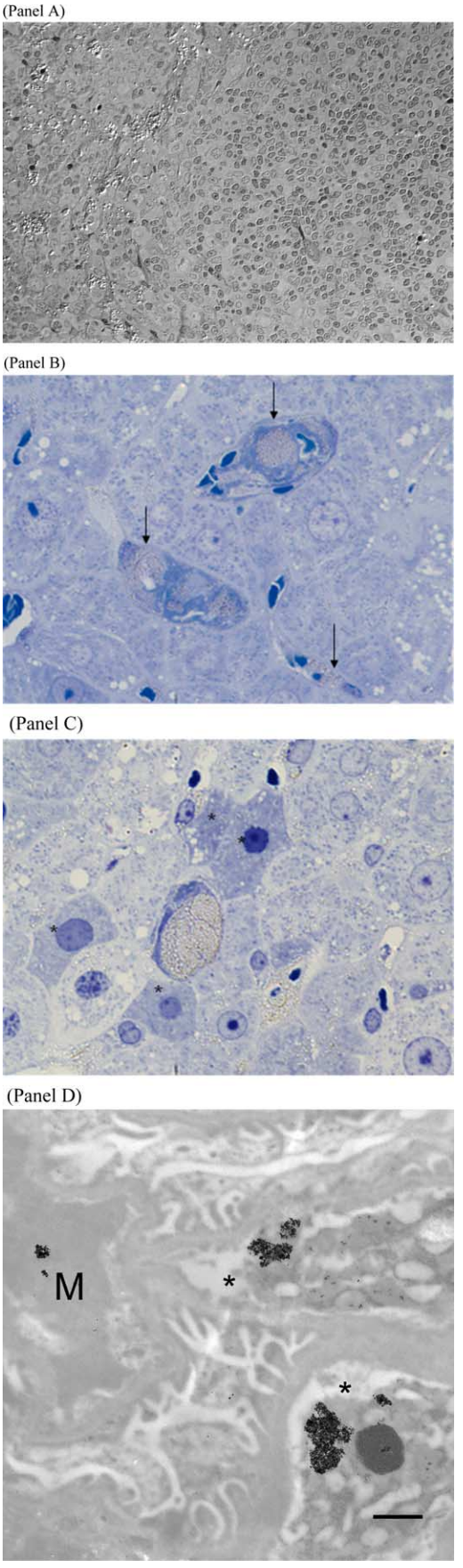


Figure 4 (Continued)

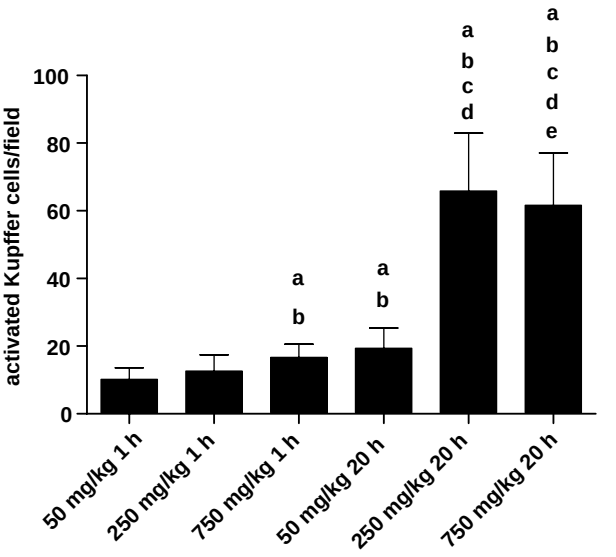


Figure 5. Activated Kupffer cell counts. Results are mean ± SD from ≥100 fields for each condition scored from 20 × (rats terminated at 20 h) or 40 × (rats terminated at 1 h) magnified images. The x axis shows the ceria dose and termination time after infusion. The rater was blind to the treatment conditions. a, b, c, d, and e = different from 50 mg/kg 1 h, 250 mg/kg 1 h, 750 mg/kg 1 h, 50 mg/kg 20 h, and 250 mg/kg 20 h treated rats, respectively.

(~10 nm, personal communication from Barry Park, Oxonica Ltd., to R. Yokel, 20 April 2007). However, ceria that exits the tailpipe is associated with soot particles, and the ceria nanoparticles have different morphologies and particle size distributions, including peaks at ~60–70 nm (HEI 2001).

As has been often reported with other nanoscale materials (Limbach et al. 2005), this nanoscale metal oxide rapidly agglomerated in the presence of sodium chloride and 10% sucrose, and *in vitro* in blood within 1 h. It would be anticipated that it would agglomerate *in vivo*, once it came into contact with blood, if the mixing of circulating blood or coating of circulating ceria by proteins did not prevent the ceria particles from coming into contact with each other. Ceria agglomerations were seen in reticuloendothelial organs. Much less ceria was seen

Figure 4. Panel A: Light micrographic image of ceria in a rat dosed with 250 mg/kg and terminated 1 h post infusion in the red pulp of spleen (left side of image), but not in the white pulp (right side of image). A similar pattern of ceria distribution was seen in rats terminated 20 h after infusion. Panel B: Light micrographic image of ceria engulfed in Kupffer cells (arrows) in a rat that received 750 mg ceria/kg and was terminated 20 h after completion of the ceria infusion. Panel C: Light micrographic image of ceria engulfed in hepatocytes in a rat that received 750 mg ceria/kg and was terminated 20 h after completion of the ceria infusion. Cellular degeneration was seen (*). Panel D: Electron micrographic image of ceria in vascular space (*) and mesangial cells (M) of the kidney in a rat that received 250 mg ceria/kg and was terminated 20 h after completion of the ceria infusion. Scale bar = 1 μm.

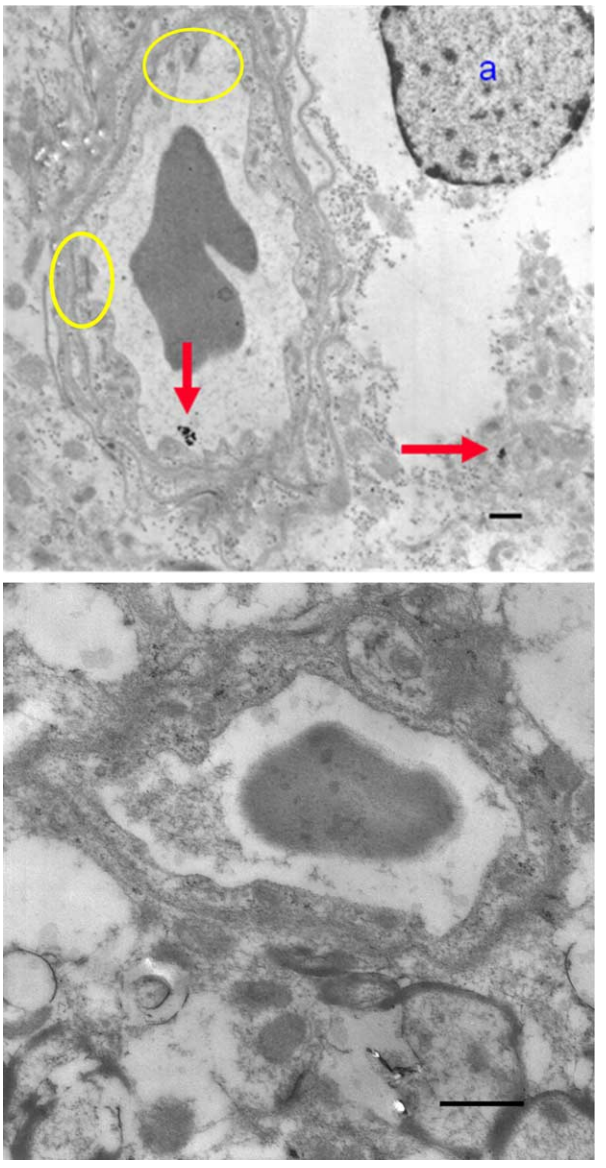


Figure 6. Upper image: Electron micrograph of hippocampus of a rat that received 750 mg ceria/kg and was terminated 20 h after the infusion. Ceria was seen in the vascular lumen (red arrows) and an astrocyte (a). The BBB appeared intact (yellow circles). Scale bar = 1 μm. Lower image: Electron micrograph of hippocampus of a rat that received 250 mg ceria/kg and was terminated 20 h after the infusion. There is an apparent absence of ceria. Scale bar = 1 μm.

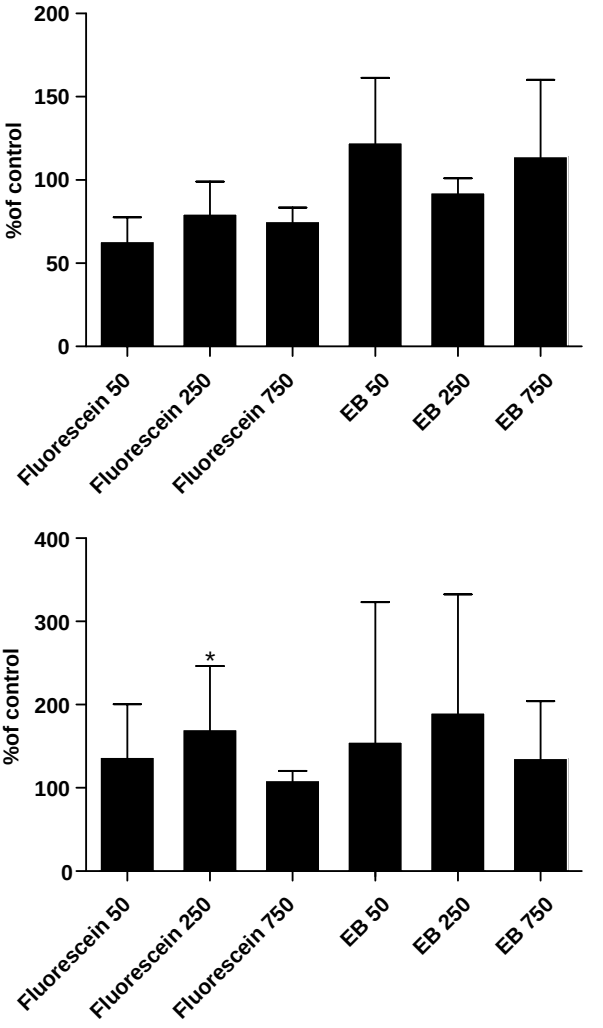


Figure 7. Brain fluorescein and Evans blue 1 h (upper panel) and 20 h (lower panel) after completion of intravenous ceria infusion. N = 4, 5, 5, and 5 rats that received 0, 50, 250 and 750 mg ceria/kg and were terminated 1 h after the infusion and 10, 7, 7, and 8 rats that received 0, 50, 250 and 750 mg ceria/kg and were terminated 20 h after the infusion. * = Significantly different from control, $p < 0.05$.

in the brain. It is not known whether the ceria agglomerated in blood and was taken up by the reticulendothelial organs as agglomerates or if the ceria agglomerates seen in the spleen, liver and kidney were formed within those organs. The circulating ceria was rapidly cleared from blood into the spleen, liver, kidney and presumably other peripheral organs. It is known that nanoscale materials that are not functionalized are rapidly cleared from circulation and that addition of PEG to the surface of ENMs prolongs residence time in circulation. However, there appear to be no prior reports of the estimated elimination half-life of centrally administered ENMs. Accumulation of nanoscale materials in reticuloendothelial organs, with the greatest mass amount cleared by the liver, has been reported after intravenous injection of 25 nm carbon particles (Biozzi et al. 1953) and 15–20 nm $^{192}$Ir particles (Kreyling et al. 2002). In the present study, ceria ENM was rapidly cleared from the blood, largely by the reticuloendothelial organs. Similarly, intravenous injection of 40 nm gold nanoparticles to mice resulted in the greatest and most rapid accumulation in Kupffer cells, with some in macrophages of the spleen, but, unlike the present results with ceria, none were found in the kidney or brain (Sadauskas et al. 2007). Localization

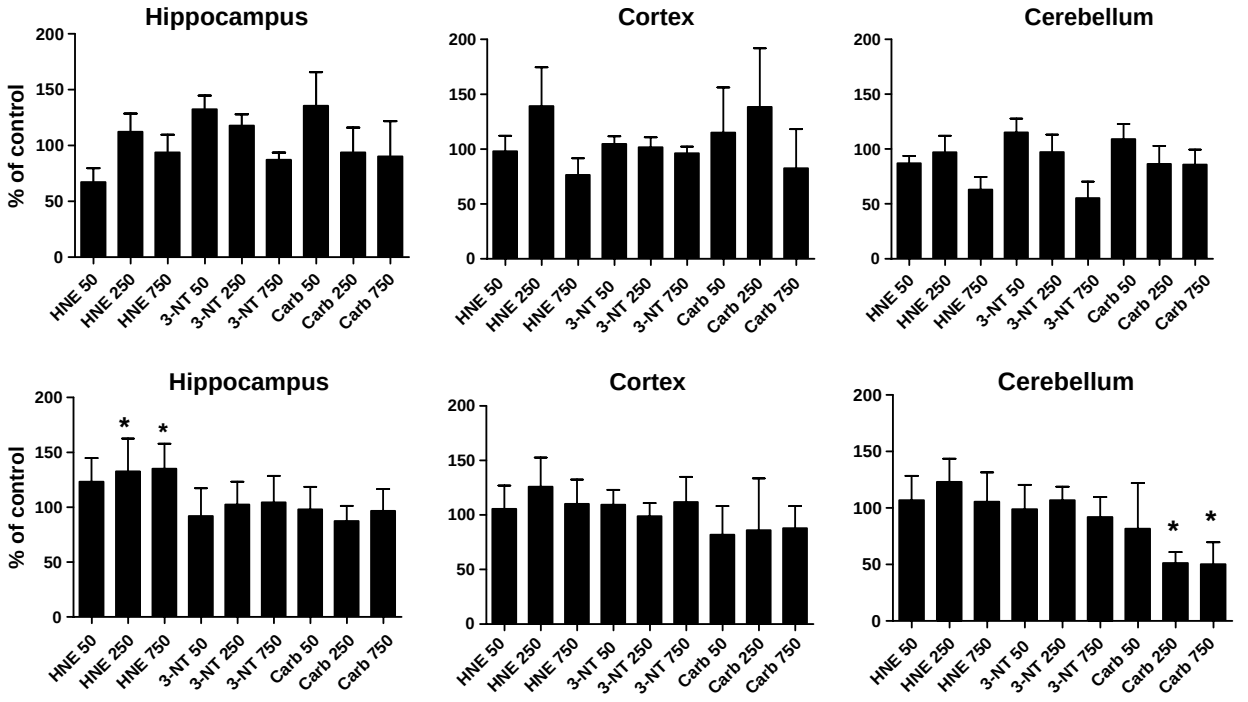


Figure 8. Protein-bound HNE, protein-bound 3-NT and protein carbonyls in the hippocampus, cortex and cerebellum 1 h (upper panels) and 20 h (lower panels) after completion of intravenous ceria ENM infusion. Results are mean ± SD of 4, 5, 5, and 5 rats that received 0, 50, 250 and 750 mg ceria/kg and were terminated 1 h after the infusion and 8, 5, 5 and 7 rats that received 0, 50, 250 and 750 mg ceria/kg and were terminated 20 h after the infusion. * = Significantly different from control, $p < 0.05$.

within the macrophages was in lysosome-like structures, suggesting to the authors uptake by endocytosis. The present results suggest no ceria redistribution out of the liver and spleen, but an increase, between 1 and 20 h. The long-term fate of these ceria agglomerations is not known. This presents the possibility of release from those organs over time. However, results of the present study up to 20 h and prior work up to seven days after inhalation and intravenous exposure to $^{192}$Ir particles suggest no significant decrease in liver content (Kreyling et al. 2002). Ce in human liver has been shown to be mainly associated with two proteins, of ~23 and 335 $kD_a$ (Chen et al. 2001). However, their identity was not determined, so it is unknown how they influence the long-term biodistribution of cerium. For low solubility 1 μm inhaled particles, such as ceria, it is estimated that, of the particles that reach circulating blood, 45% are cleared by the liver, 35% by the skeleton, 10% by other organs and the balance excreted (HEI 2001). The results of the present study are consistent with this magnitude of ceria clearance by the liver.

The reticulendothelial system is the first line of defense against xenobiotic intrusion. Thus, the spleen, liver, and kidney constitute a specific subpopulation of organs with phagocytic potential to take up ceria from systemic circulation. In the spleen, arterial circulation passes through the white pulp before entering the sinusoid of the red pulp. The macrophage-rich red pulp can become 'activated' with a few h delay (Demoy et al. 1999). This is consistent with our observation that the rats terminated after 1 h showed few ceria containing macrophages in the red pulp, while those terminated after 20 h exhibited extensive ceria laden phagocytic cells; with occasional migration into the white pulp.

The liver and spleen showed a time- and dose-dependent accumulation of ceria, indicated by the semi-quantitative EM analysis. This was supported by the quantitative Ce analysis. Given the acute nature of our study design it is not prudent to speculate on the long term consequences of the ceria ENM. It is interesting that most of the intracellular ceria appeared as cytoplasmic aggregates without showing a pattern of organelle affinity. The significance of the occasional association of ceria ENM with organelles such as mitochondria or nuclei remains to be determined. In prior work, neither 8 nm silver or 40 nm manganese particles were seen in the cell nucleus (Skebo et al. 2007). Ceria was not seen in the cell nucleus of the present work.

There was a significant activation of Kupffer cells in this study, 20 h following all doses of ceria ENM and 1 h after the highest dose. As the ceria doses used in this study were large, reflecting the low toxicity of this commercial form of ceria, Kupffer cell activation may not be seen at lower doses. However,

the trend toward greater effect from 1–20 h raises the possibility that even greater activation may occur at a later time, when lower ceria exposure might produce this effect. Activated Kupffer cells are known to be monocyte derivatives. The increase in activated Kupffer cells may reflect a heightened arrival of these blood borne cells. Alternatively, this may simply be due to activation of existing endothelially lined reticuloendothelial cells. At the present, we cannot distinguish between these possibilities.

The lack of toxicity from the intravenous administration of these large ceria doses is consistent with the understanding of ceria as an inert material. The lack of profound effects on the oxidative stress endpoints in the brain may relate to the limited ceria distribution into the brain.

No great BBB disruption was seen 1 and 20 h after completion of the infusion. Much less ceria ENM entered the brain than reticuloendothelial organs, suggesting an intact BBB during the infusion and that the BBB is an effective barrier for this crystalline ceria ENM. As it is unknown whether the ceria ENM that did enter the brain did so as administered, or after associating with proteins or other circulating factors in blood, we cannot glean from this study the properties that did enable its limited brain distribution.

Oxidative injury is a common, primary endpoint of ENM toxicity (Unfried et al. 2007). Ceria has been reported to produce toxicity attributed to increased oxidative damage (Brunner et al. 2006; Lin et al. 2006; Thill et al. 2006; Park et al. 2008).

On the other hand, ceria ENM were reported to be protective against oxidative-induced injury in cells from many origins, including the nervous system (Tarnuzzer et al. 2005; Chen et al. 2006; Schubert et al. 2006; Das et al. 2007; Niu et al. 2007; Singh et al. 2007; Xia et al. 2008). This may be a direct anti-oxidant effect of ceria owing to its ability to reversibly change from Ce(III) to Ce(IV). However, that effect was only pronounced in acidic environments (Asati et al. 2009).

The interest in ceria as a potential therapeutic agent with anti-oxidant properties increases the probability that it will be further studied for medical applications, making the understanding of its distribution from the central compartment (blood) and resultant effects important. The current study is the first report of the distribution and effects of ceria from the central compartment, after introduction into blood. However, the form of ceria employed in the present study would not be effective as a vehicle for drug delivery to the brain.

In this study, indices of protein oxidation (protein carbonyls and protein-bound 3-NT) and lipid peroxidation (protein-bound HNE) were determined. Protein carbonyls arise from at least four routes: (a) Scission of the primary amino acid backbone by reactive free radicals, forming, in the presence of paramagnetic oxygen, carbonyl functionalities; (b) oxidation of specific amino acid side chains to form, for example, oxohistidine; (c) adduction of alkenals like HNE and acrolein to Cys, His, and Lys residues by Michael addition; and (d) glycoxidation reactions in which reducing sugars that bind to Lys residues bring an aldehyde functionality with them. Modification of tyrosine residues to form 3-nitrotyrosine arises from reaction of the $NO_2$ radical with tyrosine, which has an ortho-directing OH moiety in the 4-position. This radical species, in turn, is formed by decomposition of peroxynitrite, $ONOO^-$, in the presence of $CO_2$. Peroxynitrite is formed by radical-radical reaction of NO with superoxide radical anion, with the former a product of nitric oxide synthase and the latter usually leaked from mitochondria, but also enzymatically produced (e.g., by xanthine/xanthine oxidase). Finally, HNE is formed by lipid peroxidation of unsaturated acyl chains of phospholipids, e.g., arachidonic acid. In this reaction a radical species abstracts a labile allylic H-atom from unsaturated lipid acyl chains (the β-chain of glycerophospholipids) to form a C-centered radical on the acyl chain. This immediately reacts with paramagnetic $O_2$ to form a lipid peroxyl radical, which, in turn, abstracts another labile allylic H-atom from an acyl chain on lipids to form the lipid hydroperoxide and another C-centered radical on the lipid acyl chain. This chain reaction continues. The lipid hydroperoxide can decompose into a number of products, including HNE, acrolein (2-propen-1-al), or malondialdehyde. By the well-known Michael addition reaction HNE and acrolein can bind to electron-rich S atom on Cys, or the N-atoms of His or Lys side chains to form a covalent adduct.

In the current study, we observed no alterations in any of these oxidative stress markers in brain isolated from rats 1 h after exposure to ceria ENM. Twenty h after exposure to ceria by intravenous infusion, a dose-dependent increase of protein-bound HNE in the hippocampus was observed. The hippocampus is one of the most vulnerable brain regions, and in the most common neurodegenerative disorder, Alzheimer's disease, the hippocampus, the brain area through which initial aspects of memory are formed, is severely damaged by free radicals early in the disease (Butterfield et al. 2007). The highly reactive alkenal HNE can bind to proteins, thereby inducing conformational and functional changes (Aksenov et al. 1997, 2000; Subramaniam et al. 1997; Reed et al. 2008; Perluigi et al. 2009). Hence, ceria-induced hippocampal lipid peroxidation could lead

to deficits in learning and memory, and consequently dementia. The dynamic range of increase in protein-bound HNE in brain in oxidative stress conditions, for example Alzheimer's disease, is in the order of 0–70% over control (Butterfield 1997; Butterfield and Stadtman 1997; Lauderback et al. 2001; Butterfield and Lauderback 2002; Perluigi et al. 2009). Hence, the elevated levels in brain hippocampus observed in the present study after 20 h are reflective of relatively large changes in lipid peroxidation. Such changes could have profound effects on cognitive and memory functions.

In the cerebellum, protein carbonylation was decreased compared to controls. Cerebellum is devoid of oxidative damage and other pathology in Alzheimer's disease, and though no explanation for this observation is yet known, speculation suggests that elevated levels of heme oxygenase-1 (which leads to low levels of bilirubin that are highly neuroprotective), coupled to both a different neuronal type than in hippocampus and less amyloid beta-peptide (that leads to free radical oxidative stress) accounts for this protection against oxidative stress and neurodegeneration (Poon et al. 2004). Elevated levels of heme oxygenase conceivably might be induced by ceria that lead to neuroprotection against oxidative stress as assessed by protein carbonyl levels.

The commercial ceria used in this study was not obviously accumulated in brain, perhaps because of its size as well as its propensity for agglomeration. That, nevertheless, elevated lipid peroxidation was observed in vulnerable hippocampus may reflect two possibilities: (a) Brain-resident ceria ENM induced lipid peroxidation directly, which involves a chain reaction and requires only a modest initation step to greatly amplify its effect; or (b) ceria-induced pro-inflammatory cytokines, e.g., TNF-$\alpha$, in the periphery that are well-known to cross the BBB and induce oxidative stress in brain, including lipid peroxidation (Tangpong et al. 2006, 2007; Joshi et al. 2007). Further studies will be necessary to distinguish between these or other alternatives. It is interesting to speculate that ceria ENM $<10$ nm in size, and of defined shape and surface properties, in marked contrast to what was used in the current study, might have accumulated more in brain and led to either more oxidative or more neuroprotective effects. Studies to test this notion are in progress.

In summary, ceria was rapidly cleared from the blood by peripheral reticuloendothelial tissues. Much less ceria entered the BBB cells or the brain. Ceria ENM agglomerates were seen *in vivo*, but it is not yet known if the ceria agglomerated in blood and was taken up as agglomerates or the agglomerates formed in the organs. The commercial ceria studied induced oxidative stress and a stress response in the brain. Ceria provides an inert core ENM enabling the study of the effects of size, shape and surface chemistry on the biodistribution, biotransformation and neurotoxic or neuroprotective potential of metal oxide ENMs. These results provide a foundation to study the impact of physico-chemical properties of ENMs on their brain entry and neurotoxicity or neuroprotection activity.

## Acknowledgements

The authors thank Jason Backus for his Ce analyses by ICP-AES and gratefully acknowledge the support of this work provided by the Office of the Vice President for Research, University of Kentucky, and US EPA STAR Grant RD-833772.

***Declaration of interest*:** The authors report no conflicts of interest. The authors alone are responsible for the content and writing of the paper. None of the authors has a financial conflict of interest related to this research.

## References

Asati A, Santra S, Kaittanis C, Nath S, Perez JM. 2009. Oxidase-like activity of polymer-coated cerium oxide. Angewandte Chemie 48:2308–2312.

Aksenov MY, Aksenova MV, Carney J, Butterfield DA. 1997. Oxidative modification of glutamine synthetase by amyloid beta peptide. Free Radical Res 27:267–281.

Aksenov M, Aksenova M, Butterfield DA, Markesbery WR. 2000. Oxidative modification of creatine kinase BB in Alzheimer's disease brain. J Neurochem 74:2520–2527.

Bai J, Xu Z, Zheng Y, Yin H. 2006. Shape control of $CeO_2$ nanostructure materials in microemulsion systems. Materials Lett 6:1287–1290.

Biozzi G, Benacerraf B, Halpern BN. 1953. Quantitative study of the granulopectic activity of the reticulo-endothelial system. II. A study of the kinetics of the R. E. S. in relation to the dose of carbon injected; relationship between the weight of the organs and their activity. Br J Exp Pathol 34:441–457.

Brigger I, Morizet J, Laudani L, Aubert G, Appel M, Velasco V, Terrier-Lacombe MJ, Desmaele D, d'Angelo J, Couvreur P, Vassal G. 2004. Negative preclinical results with stealth nanospheres-encapsulated Doxorubicin in an orthotopic murine brain tumor model. J Contr Release 100:29–40.

Brunner TJ, Wick P, Manser P, Spohn P, Grass RN, Limbach LK, Bruinink A, Stark WJ. 2006. *In vitro* cytotoxicity of oxide nanoparticles: Comparison to asbestos, silica, and the effect of particle solubility. Environ Sci Tech 40:4374–4381.

Butterfield DA. 1997. beta-Amyloid-associated free radical oxidative stress and neurotoxicity: implications for Alzheimer's disease. Chem Res Toxicol 10:495–506.

Butterfield DA, Stadtman ER. 1997. Protein oxidation processes in aging brain. Adv Cell Aging Gerontol 2:161–191.

Butterfield DA, Lauderback CM. 2002. Lipid peroxidation and protein oxidation in Alzheimer's disease brain: Potential causes and consequences involving amyloid b-peptide-associated free radical oxidative stress. Free Radic Biol Med 32:1050–1060.

Butterfield DA, Reed T, Newman SF, Sultana R. 2007. Roles of amyloid beta-peptide-associated oxidative stress and brain

protein modifications in the pathogenesis of Alzheimer's disease and mild cognitive impairment. Free Radic Biol Med 43:658–677.

Chen C, Zhang P, Chai Z. 2001. Distribution of some rare earth elements and their binding species with proteins in human liver studied by instrumental neutron activation analysis combined with biochemical techniques. Anal Chim Acta 439:19–27.

Chen J, Patil S, Seal S, McGinnis JF. 2006. Rare earth nanoparticles prevent retinal degeneration induced by intracellular peroxides. Nat Nanotechnol 1:142–150.

Das M, Patil S, Bhargava N, Kang JF, Riedel LM, Seal S, Hickman JJ. 2007. Auto-catalytic ceria nanoparticles offer neuroprotection to adult rat spinal cord neurons. Biomat 28:1918–1925.

Davies JC. 2006. Managing the effects of nanotechnology. Project on emerging nanotechnologies, Woodrow Wilson International Center for Scholars.

Demoy M, Andreux JP, Weingarten C, Gouritin B, Guilloux V, Couvreur P. 1999. Spleen capture of nanoparticles: Influence of animal species and surface characteristics. Pharm Res 16: 37–41.

Fenart L, Casanova A, Dehouck B, Duhem C, Slupek S, Cecchelli R, Betbeder D. 1999. Evaluation of effect of charge and lipid coating on ability of 60-nm nanoparticles to cross an in vitro model of the blood-brain barrier. J Pharmacol Exp Ther 291:1017–1022.

Feng X, Sayle DC, Wang ZL, Paras MS, Santora B, Sutorik AC, Sayle TX, Yang Y, Ding Y, Wang X, Her YS. 2006. Converting ceria polyhedral nanoparticles into single-crystal nanospheres. Science 312:1504–1508.

Ferin J, Oberdörster G, Penney DP. 1992. Pulmonary retention of ultrafine and fine particles in rats. Am J Resp Cell Mol Biol 6:535–542.

Ferin J, Oberdörster G, Penney DP, Soderholm SC, Gelein R, Piper HC. 1990. Increased pulmonary toxicity of ultrafine particles? I. Particle clearance, translocation, morphology. J Aerosol Sci 21:381–384.

Fox JL, Lamson ML. 1989. RSTRIP: Pharmacokinetic data stripping/least squares parameter optimization, MicroMath, Inc., Salt Lake City, UT, USA.

Gao K, Jiang X. 2006. Influence of particle size on transport of methotrexate across blood brain barrier by polysorbate 80-coated polybutylcyanoacrylate nanoparticles. Int J Pharmaceut 310:213–219.

Han W-Q, Wu L, Wang X, Zhu Y, Rodriguez JA. 2006. Characterization of $CeO_2$-x nanotubes by HRTEM, EELS and XANES. 231st ACS National Meeting, Atlanta, GA, USA.

Hawkins BT, Egleton RD. 2006. Fluorescence imaging of blood-brain barrier disruption. J Neurosci Meth 151:262–267.

Health Effects Institute (HEI). 2001. Evaluation of human health risk from cerium added to diesel fuel. HEI Communication 9, Boston, MA, USA.

Integrated Laboratory Systems Inc. 2006. Chemical information profile for ceric oxide [CAS No. 1306-38-3]. Supporting Nomination for Toxicological Evaluation by the National Toxicology Program. In: National Toxicology Program, NIEHS, Research Triangle Park, NC, USA; p 21.

Jakupec MA, Unfried P, Keppler BK. 2005. Pharmacological properties of cerium compounds. Rev Physiol Biochem Pharmacol 153:101–111.

Joshi G, Hardas S, Sultana R, Vore M, St Clair D, Butterfield DA. 2007. Glutathione elevation by gamma-glutamylcysteine ethyl ester as a potential therapeutic strategy towards preventing oxidative stress in brain mediated by *in vivo* administration of adriamycin: Implications for chemobrain. J Neurosci Res 85:497–503.

Kabuto M, Kubota T, Kobayashi H, Ishii H, Nakagawa T, Kawai H, Kitai R, Kodera T, Kaneko M. 1997. Experimental study of detection of brain tumor at surgery using fluorescent imaging under a surgical microscope after fluorescein administration. Brain Nerve 49:261–265.

Koziara JM, Lockman PR, Allen DD, Mumper RJ. 2006. The blood-brain barrier and brain drug delivery. J Nanosci Nanotech 6:2712–2735.

Kreyling WG, Semmler M, Erbe F, Mayer P, Takenaka S, Schulz H, Oberdörster G, Ziesenis A. 2002. Translocation of ultrafine insoluble iridium particles from lung epithelium to extrapulmonary organs is size dependent but very low. J Toxicol Environ Health A 65:1513–1530.

Lauderback CM, Hackett JM, Huang FF, Keller JN, Szweda LI, Markesbery WR, Butterfield DA. 2001. The glial transporter, GLT-1, is oxidatively modified by 4-hydroxy-2-nonenal in the Alzheimer's disease brain: Role of Ab(1-42). J Neurochem 78:413–416.

Limbach LK, Li Y, Grass RN, Brunner TJ, Hintermann MA, Muller M, Gunther D, Stark WJ. 2005. Oxide nanoparticle uptake in human lung fibroblasts: Effects of particle size, agglomeration, and diffusion at low concentrations. Environ Sci Technol 39:9370–9376.

Lin W, Huang YW, Zhou XD, Ma Y. 2006. Toxicity of cerium oxide nanoparticles in human lung cancer cells. Int J Toxicol 25:451–457.

Lockman PR, Koziara JM, Mumper RJ, Allen DD. 2004. Nanoparticle surface charges alter blood-brain barrier integrity and permeability. J Drug Targeting 12:635–641.

Lovric J, Bazzi HS, Cuie Y, Fortin GR, Winnik FM, Maysinger D. 2005. Differences in subcellular distribution and toxicity of green and red emitting CdTe quantum dots. J Mol Med 83:377–385.

Luther W. 2004. Industrial application of nanomaterials – chances and risks. Technology analysis. Future Technologies Division of VDI Technologiezentrum GmbH, Dusseldorf, Germany.

Mai H-X, Sun L-D, Zhang Y-W, Si R, Feng W, Zhang H-P, Liu H-C, Yan C-H. 2005. Shape-selective synthesis and oxygen storage behavior of ceria nanopolyhedra, nanorods and nanocubes. J Phy Chem B 109:24380–24385.

Mamot C, Nguyen JB, Pourdehnad M, Hadaczek P, Saito R, Bringas JR, Drummond DC, Hong K, Kirpotin DB, McKnight T, Berger MS, Park JW, Bankiewicz KS. 2004. Extensive distribution of liposomes in rodent brains and brain tumors following convection-enhanced delivery. J Neurooncol 68:1–9.

Maynard AD. 2006. Nanotechnology: A research strategy for addressing risk. Project on emerging nanotechnologies, Woodrow Wilson International Center for Scholars.

Nel A, Xia T, Madler L, Li N. 2006. Toxic potential of materials at the nanolevel. Science 311:622–627.

Nemmar A, Hoet PH, Vanquickenborne B, Dinsdale D, Thomeer M, Hoylaerts MF, Vanbilloen H, Mortelmans L, Nemery B. 2002. Passage of inhaled particles into the blood circulation in humans. Circulation 105:411–414.

Niu J, Azfer A, Rogers LM, Wang X, Kolattukudy PE. 2007. Cardioprotective effects of cerium oxide nanoparticles in a transgenic murine model of cardiomyopathy. Cardiovasc Res 73:549–559.

Oberdörster G, Maynard A, Donaldson K, Castranova V, Fitzpatrick J, Ausman K, Carter J, Karn B, Kreyling W, Lai D, Olin S, Monteiro-Riviere N, Warheit D, Yang H. 2005a. Principles for characterizing the potential human health effects from exposure to nanomaterials: Elements of a screening strategy. Particle Fibre Toxicol 2:35.

Oberdörster G, Oberdörster E, Oberdörster J. 2005b. Nanotoxicology: An emerging discipline evolving from studies of ultrafine particles. Environ Health Perspect 113:823–839.

Oberdörster G, Sharp Z, Atudorei V, Elder A, Gelein R, Lunts A, Kreyling W, Cox C. 2002. Extrapulmonary translocation of ultrafine carbon particles following whole-body inhalation exposure of rats. J Toxicol Environ Health A 65:1531–1543.

Park EJ, Choi J, Park YK, Park K. 2008. Oxidative stress induced by cerium oxide nanoparticles in cultured BEAS-2B cells. Toxicol 245:90–100.

Perluigi M, Sultana R, Cenini G, Di Domenico F, Memo M, Pierce WM, Coccia R, Butterfield DA. 2009. Redox proteomics identification of HNE-modified brain proteins in Alzheimer's disease: Role of lipid peroxidation in Alzheimer's disease pathogenesis. Proteomics-Clin Appl, in press.

Poon HF, Calabrese V, Scapagnini G, Butterfield DA. 2004. Free radicals: key to brain aging and heme oxygenase as a cellular response to oxidative stress. J Gerontol A Biol Sci Med Sci 59:478–493.

Qi L, Sehgal A, Castaing J-C, Chapel J-P, Fresnais J, Berret J-F, Cousin F. 2008. Redispersible hybrid nanopowders: Cerium oxide nanoparticle complexes with phosphonated-PEG oligomers. ACS Nano 2:879–888.

Reed T, Perluigi M, Sultana R, Pierce WM, Klein JB, Turner DM, Coccia R, Markesbery WR, Butterfield DA. 2008. Redox proteomic identification of 4-hydroxy-2-nonenal-modified brain proteins in amnestic mild cognitive impairment: Insight into the role of lipid peroxidation in the progression and pathogenesis of Alzheimer's disease. Neurobiol Dis 30: 107–120.

Sadauskas E, Wallin H, Stoltenberg M, Vogel U, Doering P, Larsen A, Danscher G. 2007. Kupffer cells are central in the removal of nanoparticles from the organism. Part Fibre Toxicol 4:10.

Schubert D, Dargusch R, Raitano J, Chan SW. 2006. Cerium and yttrium oxide nanoparticles are neuroprotective. Biochem Biophys Res Comm 342:86–91.

Semmler M, Seitz J, Erbe F, Mayer P, Heyder J, Oberdörster G, Kreyling WG. 2004. Long-term clearance kinetics of inhaled ultrafine insoluble iridium particles from the rat lung, including transient translocation into secondary organs. Inhal Toxicol 16:453–459.

Si R, Zhang Y-W, You L-P, Yan C-H. 2005. Rare-earth oxide nanopolyhedra, nanoplates, and nanodisks. Angewandte Chemie. Int Ed 44:3256–3260.

Singh N, Cohen CA, Rzigalinski BA. 2007. Treatment of neurodegenerative disorders with radical nanomedicine. Ann NY Acad Sci 1122:219–230.

Skebo JE, Grabinski CM, Schrand AM, Schlager JJ, Hussain SM. 2007. Assessment of metal nanoparticle agglomeration, uptake, and interaction using high-illuminating system. Int J Toxicol 26:135–141.

Subramaniam R, Roediger F, Jordan B, Mattson MP, Keller JN, Waeg G, Butterfield DA. 1997. The lipid peroxidation product, 4-hydroxy-2-trans-nonenal, alters the conformation of cortical synaptosomal membrane proteins. J Neurochem 69: 1161–1169.

Sultana R, Ravagna A, Mohmmad-Abdul H, Calabrese V, Butterfield DA. 2005. Ferulic acid ethyl ester protects neurons against amyloid beta-peptide(1-42)-induced oxidative stress and neurotoxicity: Relationship to antioxidant activity. J Neurochem 92:749–758.

Takenaka S, Karg E, Roth C, Schulz H, Ziesenis A, Heinzmann U, Schramel P, Heyder J. 2001. Pulmonary and systemic distribution of inhaled ultrafine silver particles in rats. Environ Health Perspect 109(Suppl. 4):547–551.

Tangpong J, Cole MP, Sultana R, Joshi G, Estus S, Vore M, St Clair W, Ratanachaiyavong D, St Clair D, Butterfield DA. 2006. Adriamycin-induced, TNF-mediated central nervous system toxicity. Neurobiol Dis 23:127–139.

Tangpong J, Cole MP, Sultana R, Estus S, Vore M, St Clair W, Ratanachaiyavong D, St Clair DK, Butterfield DA. 2007. Adriamycin-mediated nitration of manganese superoxide dismutase in the central nervous system: Insight into the mechanism of chemobrain. J Neurochem 100:191–201.

Tarnuzzer RW, Colon J, Patil S, Seal S. 2005. Vacancy engineered ceria nanostructures for protection from radiation-induced cellular damage. Nano Lett 5:2573–2577.

Thill A, Zeyons O, Spalla O, Chauvat F, Rose J, Auffan M, Flank AM. 2006. Cytotoxicity of $CeO_2$ nanoparticles for Escherichia coli. Physico-chemical insight of the cytotoxicity mechanism. Environ Sci Technol 40:6151–6156.

Trovarelli A. 2002. Catalysis by ceria and related materials. London: Imperial College Press.

UK MNT Network (UK Micro Nano Technology Network) Nanoscale combustion catalyst reduces diesel consumption by up to 10%. Accessed 7 March 2009 from the website: http://nanocentral.eu/uploads/downloads/nanoscalecombustion.pdf.

Unfried K, Albrecht C, Klotz L-O, von Mikecz A, Grether-Beck S, Schins RPF. 2007. Cellular responses to nanoparticles: Target structures and mechanisms. Nanotoxicology 1:52–71.

Uyama O, Okamura N, Yanase M, Narita M, Kawabata K, Sugita M. 1988. Quantitative evaluation of vascular permeability in the gerbil brain after transient ischemia using Evans blue fluorescence. J Cereb Blood Flow Metab 8:282–284.

Wang CF, Hegsted DM. 1949. Normal blood volume, plasma volume and thiocyanate space in rats and their relation to body weight. Am J Physiol 156:218–226.

Warheit DB, Borm PJ, Hennes C, Lademann J. 2007. Testing strategies to establish the safety of nanomaterials: Conclusions of an ECETOC workshop. Inhal Toxicol 19:631–643.

Xia T, Kovochich M, Liong M, Madler L, Gilbert B, Shi H, Yeh JI, Zink JI, Nel AE. 2008. Comparison of the mechanism of toxicity of zinc oxide and cerium oxide nanoparticles based on dissolution and oxidative stress properties. ACS Nano 2: 2121–2134.

Yang S, Gao L. 2006. Controlled synthesis and self-assembly of $CeO_2$ nanocubes. J Am Chem Soc 128:9330–9331.

Yu T, Joo J, Park YI, Hyeon T. 2005. Large-scale nonhydrolytic sol-gel synthesis of uniform-sized ceria nanocrystals with spherical, wire, and tadpole shapes. Angewandte Chemie, Int Ed 44:7411–7414.

Zhang F, Wang P, Koberstein J, Khalid S, Chan S-W. 2004. Cerium oxidation state in ceria nanoparticles studied with x-ray photoelectron spectroscopy and absorption near edge spectroscopy. Surface Sci 563:74–82.

This paper was first published online on iFirst on 23 May 2009.